COVER SHEET

Title: **Inverse Calculation of Displacements in CNF/PU from EIT-Imaged Conductivity Changes**

Authors: Tyler N. Tallman

ABSTRACT

Composite materials modified with carbon nanofillers have been thoroughly studied for structural health monitoring (SHM) and damage detection applications because they are piezoresistive and therefore self-sensing. That is, mechanical effects such as strain and damage collocate with conductivity changes within the material. The visualization of strain or damage-induced conductivity changes can then be leveraged for damage identification. To this end, electrical impedance tomography (EIT), has also received considerable attention for SHM because it can non-invasively image spatially-distributed conductivity changes. Despite the potential of piezoresistivity and EIT for SHM, this approach has an important limitation. EIT can only deduce conductivity changes. Conductivity, however, is not a structurally relevant parameter. From a SHM perspective, it would be much more useful to know the underlying mechanical state of the structure that gives rise to the observed conductivity changes. To achieve this, a novel piezoresistive inversion process is herein presented. This process endeavors to inversely determine the underlying displacement field of a piezoresistive material that results in an observed conductivity change as determined via EIT. The accuracy of this process is experimentally tested on a carbon nanofiber (CNF)/polyurethane (PU) nanocomposite. These preliminary results demonstrate that it is indeed possible to inversely determine the mechanical state of a body from conductivity data.

INTRODUCTION

Piezoresistive materials have recently garnered considerable attention for structural health monitoring (SHM) applications because they are self-sensing. That is, mechanical effects such as strain or damage cause local conductivity changes within the

Tyler N. Tallman, Purdue University School of Aeronautics and Astronautics, 701 W. Stadium Avenue, West Lafayette, IN 47907, U.S.A.

material. These conductivity changes can therefore be used to identify damage and deformations. Thostenson and Chou [1] showed that adding carbon nanotubes (CNTs) to the matrix phase of composite materials imparts piezoresistivity to traditionally insulating systems. Because CNTs are typically very expensive and can be difficult to disperse, other carbon-based nanofillers have also been explored for self-sensing composites such as carbon nanofibers (CNFs) and carbon black (CB).

Utilizing the piezoresistive effect for damage identification and SHM requires a method of localizing conductivity changes. For this, electrical impedance tomography (EIT) has been explored. EIT can continuously and non-invasively render images of the internal conductivity distribution of a domain. Because strain and damage collocate with conductivity changes in piezoresistive, nanofiller-modified composites, EIT can therefore locate damage or strain. This approach has been experimentally demonstrated for damage identification in composites [2] [3] [4] [5] [6] [7] [8] [9] [10] [11], damage identification in cementitious structures [12] [13] [14] [15] [16] [17], damage identification in thin films [2] [3] [18] [19] [20], strain sensing [7] [10] [20], and corrosion or saturation sensing [14] [19].

Despite the success of the preceding studies using EIT for strain and damage detection, this approach has a critical limitation. That is, EIT can only detect the occurrence of mechanical effects with no insight into the precise mechanical state that is actually giving rise to the observed conductivity change. From a SHM perspective, it would be much more beneficial to know the mechanical state of the structure. Herein, this limitation is surmounted by developing a piezoresistive inversion process. More specifically, this process inversely determines the underlying deformations of a material that result in a conductivity distribution observed by EIT. From the deformations, strains and stresses can be calculated via kinematic and constitutive relations, respectively. The piezoresistive inversion process is predicated on minimizing the difference between a conductivity distribution predicted by a piezoresistivity model and the conductivity distribution experimentally ascertained via EIT.

The remainder of this manuscript is organized as follows. First, nanocomposite piezoresistivity and the piezoresistivity modeled used in this study are briefly summarized. Next, the EIT process is presented and applied to a CNF/polyurethane (PU) nanocomposite. Then, the piezoresistive inversion process is formulated and applied to the EIT data. Finally, this manuscript ends with a brief summary and conclusions.

CARBON NANOFIBER/POLYURETHANE PIEZORESISTIVITY

In carbon nanofiller-modified composites, electrical current can propagate through the nanofiller network because electrons tunnel between sufficiently proximate nanofillers. Mechanical perturbations alter the connectedness of the nanofiller network and consequently manifest as a conductivity change. Deformations that cause nanofillers to become closer together increase conductivity whereas deformations that cause nanofillers to become further apart decrease conductivity. This corresponds to electrons having to tunnel through smaller or larger spans. Additionally, fractures that break the nanocomposite sever the network resulting in the complete cessation of conductivity at the fracture location.

Modeling piezoresistivity is an active area of research typified by several approaches including equivalent resistor network models [21], computational micromechanics models [22], and analytical models [23]. Herein, this manuscript makes use of an analytical piezoresistivity model developed previously by Tallman and Wang [23]. This model is used because its analytical formulation is readily integrated with the finite element method. This feature allows the model to predict the conductivity change of an arbitrary domain subjected to arbitrary deformations by first calculating the displacement field of the domain and then updating the conductivity of each element within the mesh based on the strain of each element. In this model, nanocomposite conductivity is predicted by the following equation originally developed by Takeda et al. [24].

$$\sigma_c = \sigma_m + \frac{4Pvl_f}{3\pi\lambda^2 d_f^2\left(\frac{4l_f}{\pi d_f^2 \sigma_f} + \frac{h^2 t}{Ae^2\sqrt{2m\varphi}}exp\left(\frac{4\pi t}{h}\sqrt{2m\varphi}\right)\right)} \tag{1}$$

In equation (1), σ_c is the nanocomposite conductivity, σ_m is the matrix conductivity, σ_f is the nanofiller conductivity, P is the percolation probability, v is the filler volume fraction, l_f is the nanofiller length, d_f is the nanofiller diameter, λ is the nanofiller waviness ratio, A is the projected area overlap between neighboring nanofillers, t is an average nanofiller-to-nanofiller distance between neighboring nanofillers, h is Planck's constant, e is the charge of an electron, and φ is the potential barrier height felt by tunneling electrons. Piezoresistivity is incorporated in this expression by identifying all of the strain-dependent parameters in equation (1), recalculating these strain-dependent parameters for a given strain state, and then recalculating equation (1) to find the strained conductivity. For the CNF/PU used in this study, $\sigma_f = 10^5$ S/m, $l_f = 11.5$ μm, and $d_f = 0.1$ μm [10]. Complete CNF/PU manufacturing details can be found in reference [10]. The nanofillers are also assumed to be straight ($\lambda = 1$) and A is assumed to be approximately equal to the cross-sectional area of the CNFs.

For this manuscript, however, a couple of important changes need to be made to the model developed by Tallman and Wang [23]. The original model was meant for linear materials and small deformations such that principal strains could be used to calculate conductivity changes. The CNF/PU, however, is mechanically nonlinear. Therefore, this manuscript instead makes use of principal stretches rather than principal strains. These changes can be summarized by replacing values of $1 + \varepsilon_i$ in the original manuscript by Tallman and Wang [23] with λ_i where ε_i is the ith principal strain and λ_i is the ith principal stretch. Second, the matrix density change due to deformation is now calculated using finite deformation metrics as $\rho = \rho_0/J$ where ρ is the current matrix density after some deformation, ρ_0 is the matrix density before deformation, and J is the determinant of the deformation gradient, F_{ij}.

ELECTRICAL IMPEDANCE TOMOGRAPHY

As discussed previously, EIT is a method of rendering an image of the internal conductivity distribution of a domain. EIT endeavors to minimize the difference between a vector of experimentally measured voltages and another vector of voltages

predicted by a numerical simulation. Mathematically, this minimization can be stated as shown in equation (2).

$$\sigma^* = \arg\min_{\sigma}\|\boldsymbol{V}_m - \boldsymbol{F}(\sigma)\|^2 \qquad (2)$$

In equation (2), σ^* is a conductivity distribution satisfying the minimization, $\boldsymbol{V}_m$ is the vector of experimentally measured voltages, and $\boldsymbol{F}(\sigma)$ is the vector of numerically predicted voltages. Note that $\boldsymbol{F}$ is explicitly written as a function of the conductivity distribution, σ. EIT operates by updating the conductivity distribution supplied to $\boldsymbol{F}$ until the minimization is satisfied. This minimization is typically approached by discretizing the domain via the finite element method. The EIT solution is therefore a mesh of piece-wise constant conductivity values. Recovering σ from equation (2) requires regularization since the inverse problem is severely ill-posed.

In this work, the soft CNF/PU was deformed by pushing three glass marbles into its surface. This experimental process is more completely described in reference [10]. The experimental setup and conductivity change predicted by EIT are shown in Figure 1. Furthermore, EIT frequently makes use of conductivity changes rather than absolute conductivity distributions since so-called difference imaging eliminates many image artifacts due to noise. That is, the domain is imaged once without any deformation and this baseline is later subtracted from the image of the conductivity during deformation. The particular EIT reconstruction presented in Figure 1 was performed on a mesh with linear hexahedral elements and three elements through the thickness. A three-dimensional mesh was used so that the three-dimensional displacements can later be ascertained from the piezoresistive inversion process. From Figure 1 it can be seen that there is a localized increase in conductivity where the marbles make contact. This can be attributed to the compressive force of the marbles causing the nanofillers in that region to become more densely packed thereby decreasing the tunneling resistance and consequently increasing the local conductivity.
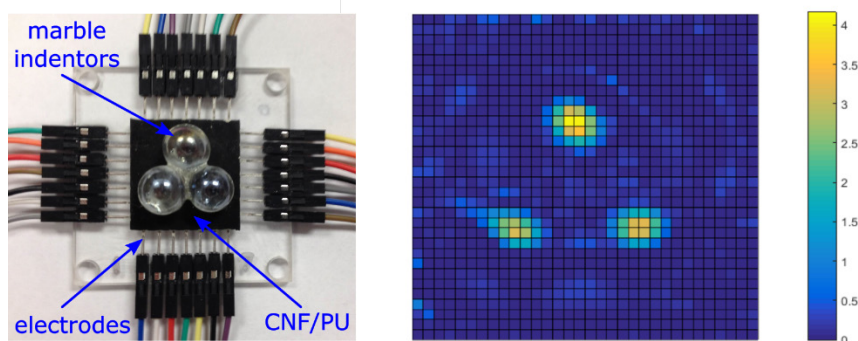

Figure 1. Left: experimental EIT setup. Right: conductivity change [S/m] rendered by EIT.

PIEZORESISTIVE INVERSION

The piezoresistive inversion process seeks a displacement field that when supplied to the previously described piezoresistivity model, produces a conductivity change matching the conductivity change imaged via EIT. In other words, the piezoresistive

inversion process wants to equate an experimentally observed conductivity change, $\delta\sigma$, and a conductivity change predicted by equation (1), $\delta\sigma_c = \sigma_c(F_{ij}) - \sigma_c(0)$. The model-predicted conductivity change, $\delta\sigma_c$, represents a change in conductivity between a zero deformation state, $\sigma_c(0)$, and a deformed state, $\sigma_c(F_{ij})$. The conductivity is expressed as a function of the deformation gradient because the previously described piezoresistivity model utilizes principal stretches which can be calculated from F_{ij}. This can more formally be stated as shown in equation (3). Here, a deformation gradient is sought to match the analytically predicted conductivity change on the right-hand side with the experimentally measured (via EIT) conductivity change on the left-hand side of equation (3).

$$\delta\sigma = \sigma_c(F_{ij}) - \sigma_c(0) \tag{3}$$

Such a deformation gradient is found by formulating a minimization problem as shown in equation (4). Now, a deformation gradient is sought that specifically minimizes the l_2-norm of the difference between $\Gamma = \delta\sigma + \sigma_c(0)$ and $\sigma_c(F_{ij})$. Here, F_{ij}^* is a deformation gradient satisfying the minimization.

$$F_{ij}^* = \arg\min_{F_{ij}} \left\| \Gamma - \sigma_c(F_{ij}) \right\|^2 \tag{4}$$

To achieve this minimization, linearize $\sigma_c(F_{ij})$ about an initial estimate of the deformation gradient, F_{ij}^0, as shown in equation (5). Upon substituting this linearization into equation (4) and defining $\delta F_{ij} = F_{ij} - F_{ij}^0$, equation (6) can be formed.

$$\sigma_c(F_{ij}) \approx \sigma_c(F_{ij}^0) + \frac{\partial\sigma_c(F_{ij}^0)}{\partial F_{ij}}(F_{ij} - F_{ij}^0) \tag{5}$$

$$F_{ij}^* = \arg\min_{F_{ij}} \left\| \Gamma - \sigma_c(F_{ij}^0) - \frac{\partial\sigma_c(F_{ij}^0)}{\partial F_{ij}}\delta F_{ij} \right\|^2 \tag{6}$$

From equation (6) δF_{ij} is found such that the initial estimate of the deformation gradient can iteratively be updated as $F_{ij}^{n+1} = F_{ij}^n + \delta F_{ij}$ until the error is sufficiently minimized where n is the nth iteration of the minimization process. To arrive at an explicit solution, equation (6) needs to be specialized to the finite element method. This can be done by replacing F_{ij} with the finite element form of the deformation gradient. After this, it is possible to find the displacement of each node belonging to the finite element mesh on which EIT was performed. Strains and stresses can also be deduced from kinematic and constitutive relations, respectively Hence, the mechanical state can inversely be determined from conductivity changes.

This process is demonstrated by making use of the previously described piezoresistivity model and EIT results on the CNF/PU. For this approach, $\partial\sigma_c/\partial F_{ij}$ is formed numerically via a two-point secant method. The results of this piezoresistive inversion are shown in Figure 2.
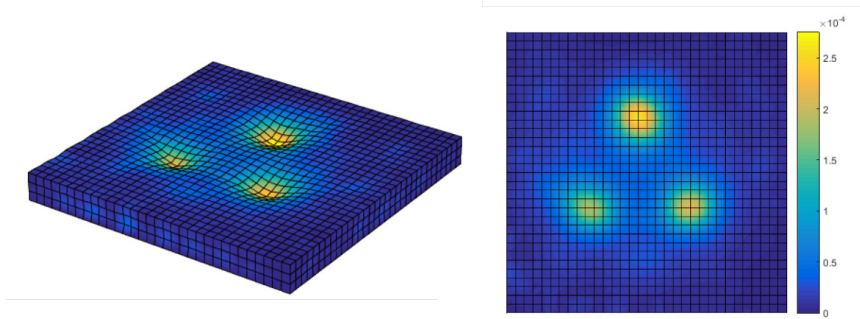
Figure 2. Magnitude of displacement field in CNF/PU predicted by piezoresistive inversion. Dimensions in meters. Left image displacements magnified by a factor of five for ease of visibility.

From Figure 2, it can be seen that the proposed piezoresistive inversion process does indeed reproduce the displacement field due to the marble indenters. A peak displacement magnitude of approximately 0.275 mm is predicted by the inversion process. Because the piezoresistive inversion process is formulated as an error minimization problem, it is important to consider the performance of equation (4). Figure 3 shows the l_2-norm of the error term for each iteration per element in the mesh. This plot represents the norm of the difference between the vector of elemental conductivity values predicted by EIT and the vector of elemental conductivity values predicted by the piezoresistivity model. As seen in Figure 3, this error norm decreases quickly and remains low for further iterations indicating that a minimum has indeed been achieved.
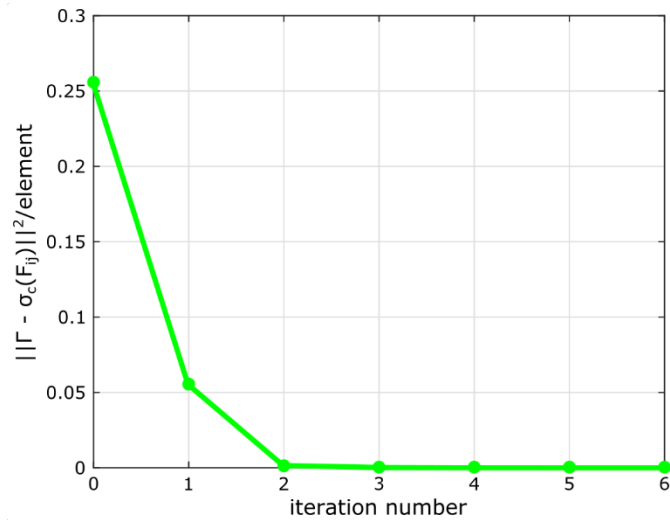

Figure 3. Error convergence for piezoresistive inversion.

SUMMARY AND CONCLUSIONS

In this manuscript, a novel piezoresistive inversion methodology to ascertain displacements from conductivity data obtained by EIT has been developed. This

inversion process is predicated on minimizing the difference between a vector of experimentally measured conductivity values and another vector of computationally predicted conductivity values. This minimization procedure works by continuously updating the deformation gradient supplied to the piezoresistivity model until the difference is minimized in the least-squares sense. Using this approach, it was demonstrated that the deformations due to three rigid indenters pushing into a much softer CNF/PU could be reproduced.

A potentially powerful aspect of this approach is that strains and stresses can be calculated from the displacements via kinematic and constitutive relations, respectively. This means that it is possible to have real-time insight into the stress state of a material as it is loaded. This insight could even be integrated with failure theories to pre-emptively predict damage and/or fractures before they occur.

In conclusion, the method developed in this manuscript seems to have considerable potential to lead to transformative integrated sensing capabilities. Because of the high temporal resolution of EIT, these results can enable the continuous determination of real time strains and stresses in piezoresistive structures. Combined with failure theories, this could enable unprecedented damage prediction and forecasting capabilities.

REFERENCES

[1] Thostenson ET, Chou TW. 2006 Carbon nanotube networks: sensing of distributed strain and damage for life prediction and self healing. *Advanced Materials.* **18**: 2837-2841.

[2] Loyola BR, Briggs TM, Arronche L, Loh KJ, La Saponara V, O'Bryan G, Skinner JL. 2013 Detection of spatially distributed damage in fiber-reinforced polymer composites. *Structural Health Monitoring.* **12**: 225-239.

[3] Loyola BR, La Saponara V, Loh KJ, Briggs TM, O'Bryan G, Skinner JL. 2013 Spatial sensing using electrical impedance tomography. *IEEE Sensors.* **13**: 2357-2367.

[4] Baltopoulos A, Polydorides N, Pambaguian L, Vavouliotis A, Kostopoulos V. 2012 Damage identification in carbon fiber reinforced polymer plates using electrical resistance tomography mapping. *Journal of Composite Materials.* **47**: 3285-3301.

[5] Baltopoulos A, Polydorides N, Pambaguian L, Vavouliotis A, Kostopoulos V. 2015 Exploiting carbon nanotube networks for damage assessment of fiber reinforced composites. *Composites Part B.* **76**: 149-158.

[6] Gallo GJ, Thostenson ET. 2015 Spatial damage detection in electrically anisotropic fiber-reinforced composites using carbon nanotube networks. *Composite Structures.* **141**: 14-23.

[7] Tallman TN, Wang KW. 2016 Damage and strain identification in multifunctional materials via electrical impedance tomography with constrained sine wave solutions. *Structural Health Monitoring.* **15**: 235-244.

[8] Tallman TN, Gungor S, Wang KW, Bakis CE. 2014 Damage detection and conductivity evolution in carbon nanofiber epoxy via electrical impedance tomography. *Smart Materials and Structures.* **23**: 045034.

[9] Tallman TN, Gungor S, Wang KW, Bakis CE. 2014 Damage detection via electrical impedance tomography in glass fiber/epoxy laminates with carbon black filler. *Structural Health Monitoring.* **14**: 100-109.

[10] Tallman TN, Gungor S, Wang KW, Bakis CE. 2015 Tactile imaging and distributed strain sensing in highly flexible carbon nanofiber/polyurethane nanocomposites. *Carbon.* **95**: 485-493.

[11] Dai H, Gallo GJ, Schumacher T, Thostenson ET. 2016 A novel methodology for spatial damage detection and imaging using a distributed carbon nanotube-based composite sensor combined with electrical impedance tomography. *Journal of Nondestructive Evaluation.* **35**: 26.

[12] Hou TC, Lynch JP. 2009 Electrical impedance tomographic methods for sensing strain fields and crack damage in cementitious structures. *Journal of Intelligent Material Systems and Structures.* **20**: 1363-1379.

[13] Hallaji M, Seppänen A, Pour-Ghaz M. 2014 Electrical impedance tomography-based sensing skin for quantitative imaging of damage in concrete. *Smart Materials and Structures.* **23**: 085001.

[14] Hallaji M, Seppänen A, Pour-Ghaz M. 2015 Electrical resistance tomography to monitor unsaturated moisture flow in cementitious materials. *Cement and Concrete Research.* **69**: 10-18.

[15] Karhunen K, Seppänen A, Lehikoinen A, Blunt J, Kaipio JP, Monteiro PJM. 2010 Electrical resistance tomography for assessment of cracks in concrete. *ACI Materials Journal.* **107**: 523-531.

[16] Karhunen K, Seppänen A, Lehikoinen A, Monteiro PJM, Kaipio JP. 2010 Electrical resistance tomography imaging of concrete. *Cement and Concrete Research.* **40**: 137-145.

[17] Gupta S, Gonzalez JG, Loh KJ. 2016 Self-sensing concrete enabled by nano-engineered cement-aggregate interfaces. *Structural Health Monitoring.* doi: 10.1007/s00466-017-1391-6.

[18] Hallaji M, Pour-Ghaz M. 2014 A new sensing skin for qualitative damage detection in concrete elements: rapid diference imaging with electrical resistance tomography. *NDT&E International.* **68**: 13-21.

[19] Hou TC, Loh KJ, Lynch JP. 2007 Spatial conductivity mapping of carbon nanotube composite thin films by electrical impedance tomography for sensing applications. *Nanotechnology.* **18**: 315501.

[20] Loh KJ, Hou TC, Lynch JP, Kotov NA. 2009 Carbon nanotube sensing skins for spatial strain and impact damage identification. *Journal of Nondestructive Evaluation.* **28**: 9-25.

[21] Gong S, Zhu ZH, Haddad EI. 2013 Modeling electrical conductivity of nanocomposites by considering carbon nanotube deformation at nanotube junctions. *Journal of Applied Physics*. **114**: 074303.

[22] Ren X, Seidel GD. 2013 Computational micromechanics modeling of inherent piezoresistivity in carbon nanotube-polymer nanocomposites. *Journal of Intelligent Material Systems and Structures.* **24**: 1459-1483.

[23] Tallman T, Wang KW. 2013 An arbitrary strains carbon nanotube composite piezoresistivity model for finite element integration. *Applied Physics Letters*. **102**: 011909.

[24] Takeda T, Shindo Y, Kuronuma Y, Narita F. 2011 Modeling and characterization of the electrical conductivity of carbon nanotube-based polymer composites. *Polymer.* **52**: 3852-3856.